

UCSF

UC San Francisco Previously Published Works

Title

Ewing sarcoma in a child with neurofibromatosis type 1

Permalink

<https://escholarship.org/uc/item/6dq2j9br>

Journal

Molecular Case Studies, 5(5)

ISSN

2373-2865

Authors

Fernandez, Karen S
Turski, Michelle L
Shah, Avanthi Tayi
[et al.](#)

Publication Date

2019-10-01

DOI

10.1101/mcs.a004580

Peer reviewed



Ewing sarcoma in a child with neurofibromatosis type 1

Karen S. Fernandez,¹ Michelle L. Turski,² Avanthi Tayi Shah,³ Boris C. Bastian,⁴ Andrew Horvai,⁵ Steven Hardee,⁶ and E. Alejandro Sweet-Cordero³

¹Division of Hematology/Oncology, Valley Children's Hospital, Madera, California 93636, USA; ²Molecular Oncology Initiative, ³Division of Hematology and Oncology, Department of Pediatrics, ⁴Departments of Dermatology and Pathology, ⁵Department of Pathology, University of California, San Francisco, San Francisco, California 94158, USA; ⁶Division of Pathology, Valley Children's Hospital, Madera, California 93636, USA

Abstract We report here on a case of Ewing sarcoma (ES) occurring in a child with neurofibromatosis type 1. The sarcoma had an *EWSR1-ERG* translocation as well as loss of the remaining wild-type allele of *NF1*. Loss of the *NF1* wild-type allele in the tumor suggests that activation of the Ras pathway contributed to its evolution. Review of available public data suggests that secondary mutations in the Ras pathway are found in ~3% of ESs. This case suggests that Ras pathway activation may play a role in tumor progression in a subset of ESs.

[Supplemental material is available for this article.]

INTRODUCTION

Ewing sarcoma (ES) is a highly malignant tumor that originates in the bone and/or soft tissue. Although it is a rare cancer with an incidence reported of anywhere from one to three people diagnosed per million in a year (Ries et al. 1999; Esiashvili et al. 2008; Potratz et al. 2012), it is the second most common primary malignancy of the bone following osteosarcoma (Esiashvili et al. 2008). The median age of diagnosis is 14–15 yr of age, although 20%–30% of cases are diagnosed in the first decade of life and cases continue to be diagnosed beyond the second decade with decreasing frequency (Bernstein et al. 2006; Potratz et al. 2012; Rochefort et al. 2017). Age is also a prognostic factor in this disease with individuals under the age of 15 having a better outcome than those 15 yr and older (PDQ Pediatric Treatment Editorial Board 2019).

Molecularly, ES is characterized by the presence of the *EWSR1* gene fusions with one of several genes from the E26 transformation-specific (ETS) family of transcription factors, such as *FLI1*, *ERG*, *ETV1*, *ETV4*, and *FEV* (Delattre et al. 1994; Burchill 2008; Grünwald et al. 2018; Nakano and Takahashi 2018). *EWSR1* is a member of the ten–eleven translocation (TET) family (Tan and Manley 2009) and in rare cases *FUS*, another member of the TET family (Tan and Manley 2009), can substitute for *EWSR1* (Gamberi et al. 2011). Additionally, there is an emerging new molecular category—Ewing-like tumor—that is morphologically similar to ES but has *EWSR1* fusions involving non-ETS genes (Renzi et al. 2019) as well as fusions with genes other than ETS or TET family members (e.g., *CIC-DUX4*, *BCOR-CCNB3*) (Cohen-Gogo et al. 2014; Specht et al. 2014). Of the *EWSR1*-ETS fusions in ES, the *EWSR1-FLI1* fusion (t(11;22)(q24;q12)) is the most commonly detected and found in 85% of cases. The *EWSR1-ERG* fusion (t(21;22)(q22;q12)) is the next most common pairing, detected in anywhere from 5% to 10% of cases (Gamberi et al. 2011).

Corresponding author:
alejandro.sweet-cordero@ucsf.edu

© 2019 Fernandez et al. This article is distributed under the terms of the Creative Commons Attribution-NonCommercial License, which permits reuse and redistribution, except for commercial purposes, provided that the original author and source are credited.

Ontology terms: Ewing's sarcoma; multiple cafe-au-lait spots; neurofibromas

Published by Cold Spring Harbor Laboratory Press

doi:10.1101/mcs.a004580

To date, there are no clinically recognized hereditary cancer syndromes that predispose individuals to ES, although it has been a topic of investigation. One group described an increased incidence of neuroectodermal tumors and stomach cancer in relatives of patients with ES, although no causative genetic factor was identified (Novakovic et al. 1994). A large case-control study that sequenced 1162 sarcoma probands, including 134 of the Ewing subtype, reported a significant association between germline mutations in FANC genes and sarcomas characterized by somatic translocations (Ballinger et al. 2016). Other reported associations of germline mutations with ES include mutations in DNA repair pathway genes such as *TP53*, *PMS2*, and others, as well as known hereditary cancer syndrome genes such as *RET*, *PTCH2*, *ATM*, and others (Zhang et al. 2015; Brohl et al. 2017). ES has also rarely been described as a second malignancy in patients with heritable retinoblastoma (Cope et al. 2001). Importantly, although these associations exist, there is little evidence demonstrating that these germline alterations played a pathogenic role in the development of ES.

Neurofibromatosis type 1 (NF-1) is an autosomal dominant hereditary cancer syndrome caused by germline loss-of-function mutations in the *NF1* gene, which encodes a RAS-GTPase-activating protein that functions as a negative regulator of Ras proteins (Cichowski and Jacks 2001). It affects one in 2500–3500 individuals worldwide irrespective of sex or ethnic background and imparts a higher risk of developing tumors (Hirbe and Gutmann 2014). NF-1 patients develop a variety of tumors by inactivation of the remaining wild-type allele of *NF1*. Almost all individuals with NF-1 will develop pigmentary skin lesions, such as café au lait macules, axillary or inguinal freckling, and/or Lisch nodules. A subset of individuals also develops skeletal abnormalities, neurologic difficulties, cardiovascular abnormalities, and/or tumors. These tumors can be malignant or benign, with benign neurofibromas occurring in 99% of individuals (Ferner 2010). The lifetime risk of cancer developing in patients with NF-1 is estimated to be ~7% (Hirbe and Gutmann 2014). Optic pathway gliomas are the most common central nervous system (CNS) tumor seen in NF-1 patients (Lewis et al. 1984), but other CNS tumors also occur (Nix et al. 2019). Additionally, non-CNS solid tumors, such as pheochromocytoma (Walther et al. 1999) and breast cancer (Sharif et al. 2007), as well as hematologic malignancies have been reported (Seminog and Goldacre 2013; Hirbe and Gutmann 2014).

A wide variety of sarcomas are associated with NF-1. Malignant peripheral nerve sheath tumors commonly occur arising from a plexiform or nodular neurofibroma. Less commonly, a wide variety of other sarcomas may occur including gastrointestinal stromal tumor (GIST) (Hurley et al. 2018), rhabdomyosarcoma (Ferrari et al. 2007), osteosarcoma, and leiomyosarcoma (Afşar et al. 2013; Kim et al. 2017). We found one report of an NF-1 patient with ES (Chowdhry et al. 2009) and another NF-1 patient with a Ewing-like sarcoma driven by a *CIC-DUX4* fusion (Tardío et al. 2015).

Here we describe a 3-yr-old child with NF-1, who was diagnosed with *EWSR1-ERG* fusion-positive ES that also harbored a somatic mutation of *NF1* in addition to a germline nonsense mutation of *NF1*. The second hit on *NF1* suggests that biallelic inactivation of *NF1* provided a growth advantage to the tumor cells and highlights the potential role of Ras pathway mutations as secondary events in ES.

RESULTS

A previously healthy, 3-yr-old girl presented with a 3-wk history of back pain and an 8-wk history of tiptoe walking. Her mother reported a clinical diagnosis of NF-1 made in Mexico; she has overt multiple neurofibromas and café au lait spots on her face and arms. The patient had not been tested for *NF1* at the time of presentation. However, on physical examination she appeared to have a clinical diagnosis of NF-1: more than six café au lait spots and axillary

freckling without overt neurofibromas (National Institutes of Health 1988). She appeared uncomfortable and was febrile with an occasional cough on initial presentation. Auscultation was notable for decreased breath sounds over the left lung. Her neurological examination showed adequate movement of the lower extremities as well as muscle tone, but she refused to stand up and walk.

A chest radiograph demonstrated two densities in the left and right paraspinal region centered around T7, measuring 3.8×2.7 cm and $5.8 \times 4.4 \times 4.5$ cm, respectively. A CT of the chest demonstrated a posterior mediastinal tumor of the mid-thoracic spine with bony destruction of T7 and tumor encroachment of the spinal cord, extending into the spinal canal from T6 to T8 (Fig. 1A–C).

A biopsy of the mass showed a highly cellular, high-grade neoplasm composed of sheets of plump spindle cells in short fascicles alternating with fibrovascular septa (Fig. 2A). The tumor cells contained scant cytoplasm, large round nuclei with vesicular chromatin and prominent nucleoli. Focal perivascular areas contained smaller round cells with conspicuous nuclear molding (Fig. 2B). Mitotic activity was brisk (more than 20 mitotic figures/10 high-power fields). Immunohistochemistry revealed the cells to be positive for synaptophysin in a perivascular distribution (Fig. 2C), whereas SOX10 was positive in scattered smaller spindle cells dispersed throughout the spindle cell areas (Fig. 2D). In addition, tumor cells were positive for vimentin, CD99 (Fig. 2F), and neuron-specific enolase (NSE) with retained BAF47 expression (not shown). Conversely, no staining for keratins, CD45, muscle-specific actin, smooth muscle actin, desmin, epithelial membrane antigen, chromogranin, or glial fibrillary acid protein (GFAP) was identified. H3K27Me3 showed a mosaic pattern of expression (Fig. 2E). Although the histology of the tumor was consistent with ES, FISH analysis of the tumor specimen showed no structural rearrangements associated with ES, although gains of

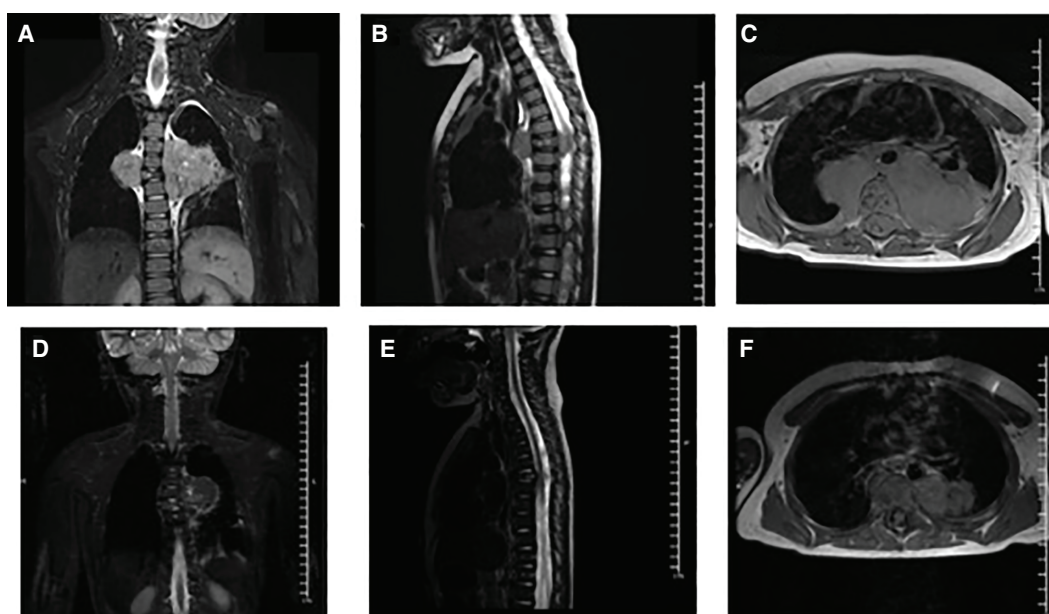


Figure 1. Diagnostic (A–C) and postinduction chemotherapy (D–F) MRI. (A) Coronal, (B) sagittal, and (C) axial views demonstrating paraspinal tumor with the displacement of the aorta and esophagus anteriorly and encroachment of the left and right hilar and bronchi as well as the left atrium and pulmonary veins. The estimated tumor volume was calculated at 720 mm^3 . (D) Coronal, (E) sagittal, and (F) axial views demonstrating good response to induction chemotherapy. Estimated tumor volume is 120 mm^3 , which represents an 84% reduction of baseline tumor size.

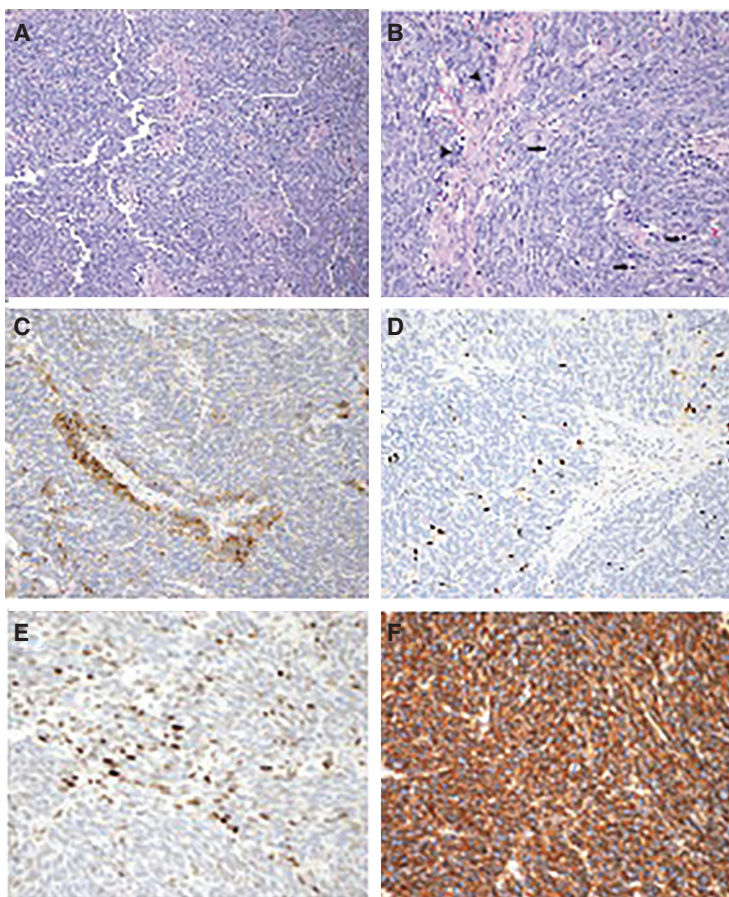


Figure 2. (A) The tumor was composed of short fascicles of plump spindle cells. (B) The tumor cells had scant cytoplasm, large nuclei with vesicular chromati, and brisk mitotic activity (arrows). Clusters of rounder cells with nuclear molding were observed around vessels (arrowhead). (C) Synaptophysin was expressed in a perivascular pattern in the round cells. (D) SOX10 showed staining in scattered smaller cells. (E) H3K27Me3 immunohistochemistry showed a patchy (so-called “mosaic”) pattern of H3K27Me3 expression. The dot-like staining in most cells represents inactivated X chromosome(s) (Schaefer et al. 2016). Multiple such signals in some nuclei may represent X-chromosome duplication. (F) CD99 expression. (A) Original magnification, 100 \times ; (B–E) original magnification, 200 \times ; (F) original magnification, 40 \times .

12q13.1 (*FOXO1*), 18q11.2 (*SS18*), and 22q12 (*EWSR1*) were observed (Supplemental Table 2). Further diagnostic classification was therefore sought by utilizing a targeted sequencing panel specifically designed to evaluate selected exons and introns for cancer-relevant genes and a subset of known fusions (Kline et al. 2017). DNA was extracted from tumor and blood. Panel testing revealed a truncating mutation of *NF1* (p.K2396*) in the tumor and an inactivating *NF1* mutation that was also present in the blood sample (p.Y2285*) (Table 1; Supplemental Fig. 1), likely resulting in biallelic inactivation of *NF1*. In addition, the tumor harbored an *EWSR1-ERG* fusion, confirming the diagnosis of ES (Table 1; Fig. 3). No other pathogenic variants were detected in the submitted tumor specimen.

Pending sequencing results, Ewing therapy with concurrent radiation therapy was started after surgical resection of the tumor using an interval-compression chemotherapy consisting of vincristine, doxorubicin, and cyclophosphamide alternating with ifosfamide and etoposide given the tumor histologically appeared to be consistent with ES and because of the rapidly evolving cord compression. The patient tolerated chemotherapy well and after

Table 1. Variant table

Gene	Chr	HGVS DNA reference	HGVS protein reference	Variant type	Predicted effect	dbSNP/dbVar ID	Genotype or allele frequency	ClinVar ID
Blood sample								
<i>NF1</i>	17	c.6855C>A	p.Y2285*	Nonsense	Pathogenic	rs772295894	Heterozygous	185082
Tumor tissue								
<i>NF1</i>	17	c.7186A>T	p. K2396*	Nonsense	Pathogenic	Not reported	37% allele frequency	Not reported
<i>NF1</i>		c.6855C>A	p.Y2285*	Nonsense	Pathogenic	rs772295894	57% allele frequency	185082
<i>EWSR1, ERG</i>	22, 21	t(21;22)(q22;q12)	EWSR1-ERG	Fusion	Pathogenic	Not applicable	Not available	Not reported

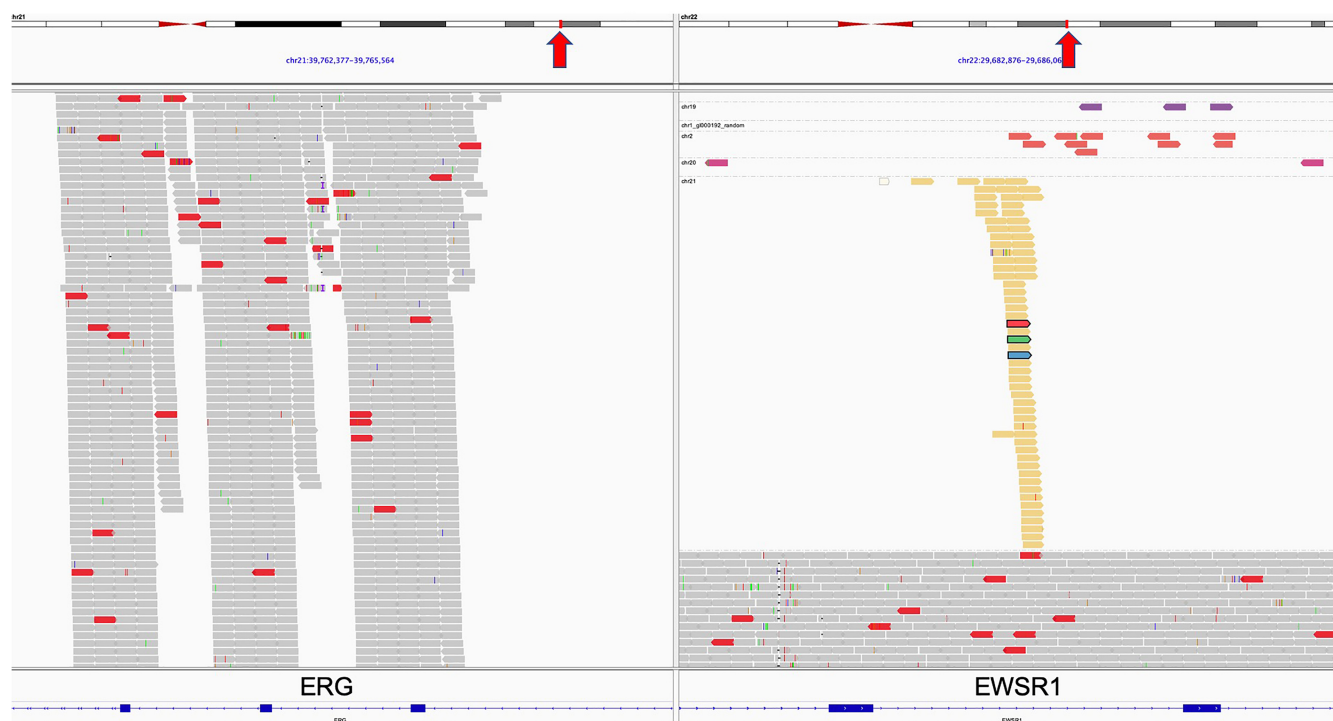


Figure 3. Integrated Genome Viewer snapshot of the chimeric read pairs mapping to intron 7 of *ERG* on Chromosome 21 (genomic position indicated by red arrow at ideogram at top) and intron 8 of *EWSR1* and on Chromosome 22 (genomic position indicated by red arrow at ideogram at top). The blue boxes at the bottom indicate the position of exons 6, 7, and 8 of *ERG* and 8 and 9 of *EWSR1*. The sequencing assay tiles over introns 5–13 of *EWSR1* and all its exons. Only exons of *ERG* are captured and are not shown in the left panel because of the height of the chimeric read pile over *ERG* intron 7. Reads are colored by insert size. The gray reads over *EWSR1* at the bottom of the right panel show the unrearranged background reads over the captured region of *EWSR1*.

two cycles of chemotherapy the tiptoe walking resolved. Evaluation of response at the end of six cycles of induction chemotherapy showed dramatic improvement in the intraspinal tumor. Measurements of the right and left paraspinous thoracic tumor showed a >80% decrease in volume compared to baseline (Fig. 1D–F). The patient completed treatment and is currently doing well 3 mo after completion of therapy.

DISCUSSION

Ewing sarcoma in patients with NF-1 has been reported only once in the literature (Chowdhry et al. 2009), although in that report there was no characterization of the type of ES fusion or *NF1* mutations. In the case reported here, an *EWSR1-ERG* fusion was detected by a next-generation sequencing (NGS) assay but not by FISH. False-negative results using dual break-apart probes for the detection of the *EWSR1-ERG* fusion can occur because of the complex nature of this rearrangement (Chen et al. 2016).

Mechanistically, *EWSR1-ETS* fusions exert their oncogenic affect by driving dramatic changes in the transcriptome of cells harboring the fusion (Erkizan et al. 2010). Receptor tyrosine kinases (RTKs) have been shown to have higher transcript expression levels in ES tumors (Potratz et al. 2016), and as the Ras pathway is a major effector of downstream signaling for RTKs, it may represent an important mediator of the oncogenic effects of *EWSR1* fusions. *IGFR1* is a well-established RTK that has been shown to be essential in this capacity (Gaspar et al. 2012). In support of this, inhibition of the Ras pathway through MEK1/2 inhibitors has been shown to suppress malignant phenotypes in ES cell lines (Silvany et al. 2000; Benini et al. 2004). Additionally, two independent studies reported down-regulation of *SPRY1* and miRNA *let-7*, both negative regulators of RAS, in ES cell lines resulting in Ras pathway activation (Hameiri-Grossman et al. 2015; Cidre-Aranaz et al. 2017). It is interesting to speculate that as Ras is a main converging point for downstream signaling of activated RTKs up-regulated in ES, the acquisition of mutations or implementation of other molecular mechanisms that can result in Ras pathway activation may be advantageous to ES cells. NF1 is one such target as it is a negative regulator of the Ras pathway, where it catalyzes the hydrolysis of Ras-bound guanosine triphosphate (GTP) to guanine diphosphate (GDP) and keeps Ras in the active state (Cichowski and Jacks 2001).

The patient presented here had two *NF1* mutations. The germline *NF1* p.Y2285* (c.6855C>A) found in the patient described here is a known pathogenic variant associated with NF-1 (Table 1; ClinVar ID 185082). The somatic nonsense mutation p.K2396* seen in this patient has been reported in a single sample of a grade IV astrocytoma (COSM5766195). It is not present in ClinVar or LOVD but is predicted to result in protein truncation and classified as a PVS1 according to ACMG guidelines (Richards et al. 2015). The two nonsense mutations affected different exons so that they could not be phased. However, we also observed a large deletion of Chromosome 17, where *NF1* resides in the tumor (Fig. 4). One possible explanation for this observation is that the tumor is polyploid and duplicate copies of the wild-type *NF1* gene were removed by two independent events—the tumor-specific p.K2396* mutation and loss of a chromosome. Although polyploidy was originally suggested by the *EWSR1* FISH results showing copy-number increase of the locus (Supplemental Table 2), chromosome analysis (Supplemental Fig. 2) subsequently revealed a normal female complement with no abnormal clones detected. An alternative explanation is the presence of heterogeneity in the tumor. The second hit somatic mutation in *NF1* was present at an allele frequency of 37%, which could suggest a subclonal nature to this mutation. Although not definitive, the two nonsense mutations in *NF1* in conjunction with the Chromosome 17 deletion encompassing *NF1* favor a model of biallelic inactivation and reduces the likelihood that NF1 inactivation is happening by chance in this tumor; biallelic

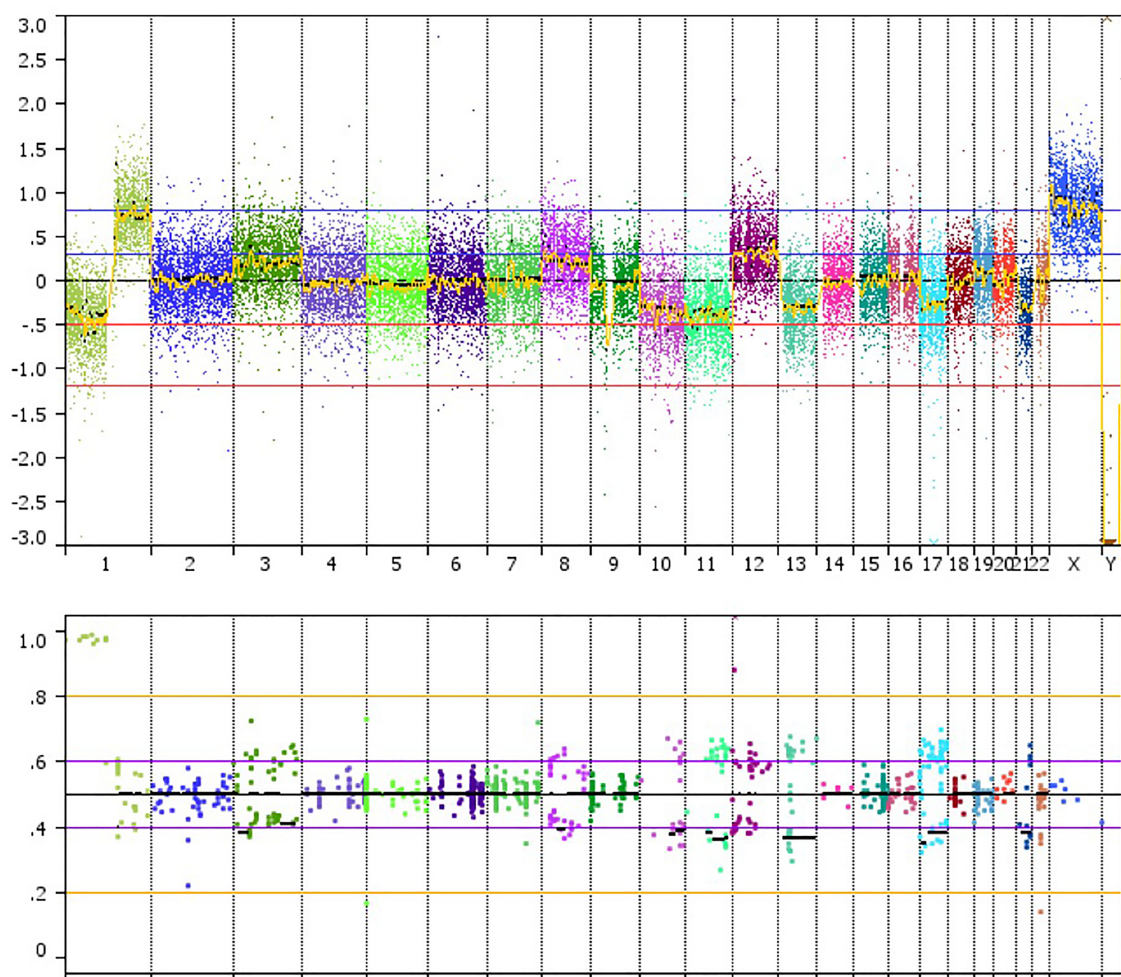


Figure 4. Genome-wide copy-number changes. The y-axis shows the log₂ ratio of normalized ratio of copy-number changes in the tumor to a reference genome with 0 corresponding to no copy-number change. The x-axis shows the genome from Chromosome 1 to Chromosome Y. The *upper* panel shows the copy number across the genome; the *lower* panel shows the variant allele frequency.

inactivation of *NF1* suggests that there was a selective advantage to losing the wild-type allele and that *NF1* is contributing to sarcomagenesis.

Mutations in Ras pathway genes have only infrequently been reported in ES (Shukla et al. 2012; Zhang et al. 2016). Querying the GENIE cBioPortal database (v5.0) confirmed the paucity of Ras pathway mutations in ES, with only four cases of 143 ES patients in whose tumors mutated Ras pathway genes were detected (AACR Project GENIE Consortium 2017).

This case highlights several important aspects of the evaluation of solid tumors and the role of NGS analysis in their evaluation. First, it demonstrates that NGS can sometimes identify pathogenic fusion events not detected by standard methods. In this particular case, NGS testing was used to confirm the diagnosis of ES. This highlights the potential utility of NGS, although it should be noted that access to this technology continues to be limited, especially in middle- and low-income countries. Other immunohistochemistry-based tests may be useful for confirming ES in patients (Baldauf et al. 2018). Second, it demonstrates the utility of

NGS analysis in tumors from patients with inherited cancer predispositions, as it can evaluate the role of the inherited predisposition in the pathogenesis of specific cancer under study. In the case reported here, NGS clearly demonstrated a likely role for the inherited predisposition because the tumor acquired a second hit in the same gene. Last, this case underscores the underappreciated role of the Ras pathway in the pathogenesis and progression of ES.

METHODS

NGS Testing

Genomic DNA was extracted from tumor tissue that had been macrodissected from formalin-fixed, paraffin-embedded blocks and blood. Capture-based next-generation DNA sequencing was performed as previously described at the UCSF Clinical Cancer Genomics Laboratory, using an assay that targets all coding exons of 479 cancer-related genes, *TERT* promoter, select introns, and upstream regulatory regions of 47 genes (Supplemental Table 1) to enable detection of structural variants including gene fusions and DNA segments at regular intervals along each chromosome to enable genome-wide copy-number and zygosity analysis, with a total sequencing footprint of 2.8 Mb. Sequencing libraries were prepared from genomic DNA, and target enrichment was performed by hybrid capture using a custom oligonucleotide library (Roche NimbleGen). Sequencing was performed on an Illumina HiSeq 2500. Tumors are sequenced to an average unique depth coverage of approximately $>500\times$. Duplicate sequencing reads were removed computationally to allow for accurate allele frequency determination and copy-number calling. The analysis was based on the human reference sequence (NCBI build 37) using the following software packages: BWA 0.7.13, Samtools 1.1 (using htlib 1.1), Picard tools 1.97 (1504), GATK Appistry v2015.1.1-3.4.46-0-ga8e1d99, CNVkit 0.7.2, Pindel 0.2.5b8, SATK Appistry v2015.1.1-1-gea45d62, ANNOVAR v2016Feb01, FreeBayes 0.9.20, and Delly 0.7.2.13-20 Single-nucleotide variants, insertions/deletions, and structural variants were visualized and verified using the Integrated Genome Viewer. Genome-wide copy-number analysis based on on-target and off-target reads was performed by CNVkit (Talevich et al. 2016) and visualized with Nexus Copy Number (Biodiscovery). See Supplemental Table 3 for sequencing coverage details.

FISH Testing

FISH testing was performed by the Pathology Department at Valley Children's Hospital in Madera, California according to standard protocols. Probes for detecting the EWSR1 fusion were from Abbott Molecular.

Histopathology

Four micrometer sections of formalin-fixed paraffin-embedded tissue were stained with hematoxylin and eosin. Immunostaining and detection were performed on a Leica Bond III automated immunostainer using primary antibodies, clones, dilutions and sources, respectively: synaptophysin (polyclonal; 1:100, Cell-Marque), SOX10 (EP268, 1:250 Cell-Marque), CD99 (EPR3097Y, 1:100, Cell-Marque), H3K27Me3 (C36B11, 1:50, Cell Signaling Technology). Synaptophysin was done to investigate the presence of neuroendocrine differentiation—SOX10 for nerve sheath/melanocytic differentiation and CD99 as a sensitive, but not specific, stain for ES.

ADDITIONAL INFORMATION

Data Deposition and Access

Raw sequencing data were not deposited but are available from the authors on reasonable request. The *NF1* and *EWSR1-ERG* variants described in this study were submitted to ClinVar (<http://www.ncbi.nlm.nih.gov/clinvar/>) and can be found under accession numbers SCV000993588–SCV000993590.

Competing Interest Statement

The authors have declared no competing interest.

Referees

Antonio Llombart Bosch
Anonymous

Received June 30, 2019;
accepted in revised form
August 28, 2019.

Ethics Statement

Verbal consent was obtained from the mother of this patient to publish this article. The verbal consent was obtained in Spanish by Dr. Alejandro Sweet-Cordero and witnessed by Dr. Avanthi Shah, who are both fluent in Spanish and authors of this manuscript. The patient is directly cared for by another author of this manuscript (Dr. Fernandez), who also obtained consent from the mother verbally for sharing of this information. We have IRB consent for registry of cases sequenced by our CLIA-certified assay (University of California, San Francisco IRB 18-24582).

REFERENCES

- AACR Project GENIE Consortium. 2017. AACR Project GENIE: powering precision medicine through an international consortium. *Cancer Discov* **7**: 818–831. doi:10.1158/2159-8290.CD-17-0151
- Afşar CU, Kara IO, Kozat BK, Demiryürek H, Duman BB, Doran F. 2013. Neurofibromatosis type 1, gastrointestinal stromal tumor, leiomyosarcoma and osteosarcoma: four cases of rare tumors and a review of the literature. *Crit Rev Oncol Hematol* **86**: 191–199. doi:10.1016/j.critrevonc.2012.11.001
- Baldauf MC, Orth MF, Dallmayer M, Marchetto A, Gerke JS, Rubio RA, Kiran MM, Musa J, Knott MML, Ohmura S, et al. 2018. Robust diagnosis of Ewing sarcoma by immunohistochemical detection of super-enhancer-driven *EWSR1-ETS* targets. *Oncotarget* **9**: 1587–1601. doi:10.18632/oncotarget.20098
- Ballinger ML, Goode DL, Ray-Coquard I, James PA, Mitchell G, Niedermayr E, Puri A, Schiffman JD, Dite GS, Cipponi A, et al. 2016. Monogenic and polygenic determinants of sarcoma risk: an international genetic study. *Lancet Oncol* **17**: 1261–1271. doi:10.1016/S1470-2045(16)30147-4
- Benini S, Manara MC, Cerisano V, Perdichizzi S, Strammiello R, Serra M, Picci P, Scotlandi K. 2004. Contribution of MEK/MAPK and PI3-K signaling pathway to the malignant behavior of Ewing's sarcoma cells: therapeutic prospects. *Int J Cancer* **108**: 358–366. doi:10.1002/ijc.11576
- Bernstein M, Kovar H, Paulussen M, Randall RL, Schuck A, Teot LA, Juergens H. 2006. Ewing's sarcoma family of tumors: current management. *Oncologist* **11**: 503–519. doi:10.1634/theoncologist.11-5-503
- Brohl AS, Patidar R, Turner CE, Wen X, Song YK, Wei JS, Calzone KA, Khan J. 2017. Frequent inactivating germline mutations in DNA repair genes in patients with Ewing sarcoma. *Genet Med* **19**: 955–958. doi:10.1038/gim.2016.206
- Burchill SA. 2008. Molecular abnormalities in Ewing's sarcoma. *Expert Rev Anticancer Ther* **8**: 1675–1687. doi:10.1586/14737140.8.10.1675
- Chen S, Deniz K, Sung Y-S, Zhang L, Dry S, Antonescu CR. 2016. Ewing sarcoma with *ERG* gene rearrangements: a molecular study focusing on the prevalence of *FUS-ERG* and common pitfalls in detecting *EWSR1-ERG* fusions by FISH. *Genes Chromosomes Cancer* **55**: 340–349. doi:10.1002/gcc.22336
- Chowdhry M, Hughes C, Grimer RJ, Sumathi V, Wilson S, Jeys L. 2009. Bone sarcomas arising in patients with neurofibromatosis type 1. *J Bone Joint Surg Br* **91**: 1223–1226. doi:10.1302/0301-620X.91B9.22299
- Cichowski K, Jacks T. 2001. NF1 tumor suppressor gene function: narrowing the GAP. *Cell* **104**: 593–604. doi:10.1016/S0092-8674(01)00245-8
- Cidre-Aranaz F, Grünwald TGP, Surdez D, García-García L, Carlos Lázaro J, Kirchner T, González-González L, Sastre A, García-Miguel P, López-Pérez SE, et al. 2017. EWS-FLI1-mediated suppression of the RAS-antagonist Sprouty 1 (SPRY1) confers aggressiveness to Ewing sarcoma. *Oncogene* **36**: 766–776. doi:10.1038/onc.2016.244
- Cohen-Gogo S, Cellier C, Coindre J-M, Mosseri V, Pierron G, Guillemet C, Italiano A, Brugières L, Orbach D, Laurence V, et al. 2014. Ewing-like sarcomas with *BCOR-CCNB3* fusion transcript: a clinical, radiological and pathological retrospective study from the Société Française des Cancers de L'Enfant. *Pediatr Blood Cancer* **61**: 2191–2198. doi:10.1002/pbc.25210

- Cope JU, Tsokos M, Miller RW. 2001. Ewing sarcoma and sinonasal neuroectodermal tumors as second malignant tumors after retinoblastoma and other neoplasms. *Med Pediatr Oncol* **36**: 290–294. doi:10.1002/1096-911X(20010201)36:2<290::AID-MPO1067>3.0.CO;2-5
- Delattre O, Zucman J, Melot T, Garau XS, Zucker JM, Lenoir GM, Ambros PF, Sheer D, Turc-Carel C, Triche TJ. 1994. The Ewing family of tumors—a subgroup of small-round-cell tumors defined by specific chimeric transcripts. *N Engl J Med* **331**: 294–299. doi:10.1056/NEJM199408043310503
- Erkizan HV, Uversky VN, Toretsky JA. 2010. Oncogenic partnerships: EWS-FLI1 protein interactions initiate key pathways of Ewing's sarcoma. *Clin Cancer Res* **16**: 4077–4083. doi:10.1158/1078-0432.CCR-09-2261
- Esiashvili N, Goodman M, Marcus RB. 2008. Changes in incidence and survival of Ewing sarcoma patients over the past 3 decades: surveillance epidemiology and end results data. *J Pediatr Hematol Oncol* **30**: 425–430. doi:10.1097/MPH.0b013e31816e22f3
- Ferner RE. 2010. The neurofibromatoses. *Pract Neurol* **10**: 82–93. doi:10.1136/jnnp.2010.206532
- Ferrari A, Bisogno G, Macaluso A, Casanova M, D'Angelo P, Pierani P, Zanetti I, Alaggio R, Cecchetto G, Carli M. 2007. Soft-tissue sarcomas in children and adolescents with neurofibromatosis type 1. *Cancer* **109**: 1406–1412. doi:10.1002/cncr.22533
- Gamberi G, Cocchi S, Benini S, Magagnoli G, Morandi L, Kreshak J, Gambarotti M, Picci P, Zanella L, Alberghini M. 2011. Molecular diagnosis in Ewing family tumors: the Rizzoli experience—222 consecutive cases in four years. *J Mol Diagn* **13**: 313–324. doi:10.1016/j.jmoldx.2011.01.004
- Gaspar N, Di Giannatale A, Geoerger B, Redini F, Corradini N, Enz-Werle N, Tirode F, Marec-Berard P, Gentet J-C, Laurence V, et al. 2012. Bone sarcomas: from biology to targeted therapies. *Sarcoma* **2012**: 301975. doi:10.1155/2012/301975
- Grünewald TGP, Cidre-Aranaz F, Surdez D, Tomazou EM, de Álava E, Kovar H, Sorensen PH, Delattre O, Dirksen U. 2018. Ewing sarcoma. *Nat Rev Dis Primers* **4**: 5. doi:10.1038/s41572-018-0003-x
- Hameiri-Grossman M, Porat-Klein A, Yaniv I, Ash S, Cohen IJ, Kodman Y, Haklai R, Elad-Sfadia G, Kloog Y, Chepurko E, et al. 2015. The association between let-7, RAS and HIF-1 α in Ewing Sarcoma tumor growth. *Oncotarget* **6**: 33834–33848. doi:10.18632/oncotarget.5616
- Hirbe AC, Gutmann DH. 2014. Neurofibromatosis type 1: a multidisciplinary approach to care. *Lancet Neurol* **13**: 834–843. doi:10.1016/S1474-4422(14)70063-8
- Hurley RH, McCormick M, Elhassan M, Nicholson G. 2018. Gastrointestinal stromal tumour as a rare association with neurofibromatosis type 1. *J Surg Case Rep* **2018**: rjy017. doi:10.1093/jscr/rjy017
- Kim A, Stewart DR, Reilly KM, Viskochil D, Miettinen MM, Widemann BC. 2017. Malignant peripheral nerve sheath tumors state of the science: leveraging clinical and biological insights into effective therapies. *Sarcoma* **2017**: 7429697. doi:10.1155/2017/7429697
- Kline CN, Joseph NM, Grenert JP, van Ziffle J, Talevich E, Onodera C, Aboian M, Cha S, Raleigh DR, Braunstein S, et al. 2017. Targeted next-generation sequencing of pediatric neuro-oncology patients improves diagnosis, identifies pathogenic germline mutations, and directs targeted therapy. *Neuro Oncol* **19**: 699–709. doi:10.1093/neuonc/now254
- Lewis RA, Gerson LP, Axelson KA, Riccardi VM, Whitford RP. 1984. von Recklinghausen neurofibromatosis. II. Incidence of optic gliomata. *Ophthalmology* **91**: 929–935. doi:10.1016/S0161-6420(84)34217-8
- Nakano K, Takahashi S. 2018. Translocation-related sarcomas. *Int J Mol Sci* **19**: E3784. doi:10.3390/ijms19123784
- National Institutes of Health. 1988. Neurofibromatosis. Conference statement. National Institutes of Health Consensus Development Conference. *Arch Neurol* **45**: 575–578. doi:10.1001/archneur.1988.00520290115023
- Nix JS, Blakeley J, Rodriguez FJ. 2019. An update on the central nervous system manifestations of neurofibromatosis type 1. *Acta Neuropathol* doi:10.1007/s00401-019-02002-2
- Novakovic B, Goldstein AM, Wexler LH, Tucker MA. 1994. Increased risk of neuroectodermal tumors and stomach cancer in relatives of patients with Ewing's sarcoma family of tumors. *J Natl Cancer Inst* **86**: 1702–1706. doi:10.1093/jnci/86.22.1702
- PDQ Pediatric Treatment Editorial Board. 2019. *Ewing sarcoma treatment*. <https://www.ncbi.nlm.nih.gov/books/NBK66045/>
- Potratz J, Dirksen U, Jürgens H, Craft A. 2012. Ewing sarcoma: clinical state-of-the-art. *Pediatr Hematol Oncol* **29**: 1–11. doi:10.3109/08880018.2011.622034
- Potratz J, Tillmanns A, Berning P, Korsching E, Schaefer C, Lechtape B, Schleithoff C, Unland R, Schäfer K-L, Müller-Tidow C, et al. 2016. Receptor tyrosine kinase gene expression profiles of Ewing sarcomas reveal ROR1 as a potential therapeutic target in metastatic disease. *Mol Oncol* **10**: 677–692. doi:10.1016/j.molonc.2015.12.009
- Renzi S, Anderson ND, Light N, Gupta A. 2019. Ewing-like sarcoma: an emerging family of round cell sarcomas. *J Cell Physiol* **234**: 7999–8007. doi:10.1002/jcp.27558

- Richards S, Aziz N, Bale S, Bick D, Das S, Gastier-Foster J, Grody WW, Hegde M, Lyon E, Spector E, et al. 2015. Standards and guidelines for the interpretation of sequence variants: a joint consensus recommendation of the American College of Medical Genetics and Genomics and the Association for Molecular Pathology. *Genet Med* **17**: 405–424. doi:10.1038/gim.2015.30
- Ries L, Smith M, Gurney J, Linet M, Tamra T, Young J, Bunin G. 1999. *Cancer incidence and survival among children and adolescents, United States SEER Program 1975–1995*. National Cancer Institute, SEER Program, Bethesda, MD.
- Rocheftort P, Italiano A, Laurence V, Penel N, Lardy-Cleaud A, Mir O, Chevreau C, Bertucci F, Bompas E, Chaigneau L, et al. 2017. A retrospective multicentric study of Ewing sarcoma family of tumors in patients older than 50: management and outcome. *Sci Rep* **7**: 17917. doi:10.1038/s41598-017-17733-z
- Schaefer I-M, Minkovsky A, Hornick JL. 2016. H3K27me3 immunohistochemistry highlights the inactivated X chromosome (Xi) and predicts sex in non-neoplastic tissues. *Histopathology* **69**: 702–704. doi:10.1111/his.12972
- Seminog OO, Goldacre MJ. 2013. Risk of benign tumours of nervous system, and of malignant neoplasms, in people with neurofibromatosis: population-based record-linkage study. *Br J Cancer* **108**: 193–198. doi:10.1038/bjc.2012.535
- Sharif S, Moran A, Huson SM, Iddenden R, Shenton A, Howard E, Evans DGR. 2007. Women with neurofibromatosis 1 are at a moderately increased risk of developing breast cancer and should be considered for early screening. *J Med Genet* **44**: 481–484. doi:10.1136/jmg.2007.049346
- Shukla N, Ameer N, Yilmaz I, Nafa K, Lau C-Y, Marchetti A, Borsu L, Barr FG, Ladanyi M. 2012. Oncogene mutation profiling of pediatric solid tumors reveals significant subsets of embryonal rhabdomyosarcoma and neuroblastoma with mutated genes in growth signaling pathways. *Clin Cancer Res* **18**: 748–757. doi:10.1158/1078-0432.CCR-11-2056
- Silvany RE, Eliazar S, Wolff NC, Ilaria RL. 2000. Interference with the constitutive activation of ERK1 and ERK2 impairs EWS/FLI-1-dependent transformation. *Oncogene* **19**: 4523–4530. doi:10.1038/sj.onc.1203811
- Specht K, Sung Y-S, Zhang L, Richter GHS, Fletcher CD, Antonescu CR. 2014. Distinct transcriptional signature and immunoprofile of *CIC-DUX4* fusion-positive round cell tumors compared to *EWSR1*-rearranged Ewing sarcomas: further evidence toward distinct pathologic entities. *Genes Chromosomes Cancer* **53**: 622–633. doi:10.1002/gcc.22172
- Talevich E, Shain AH, Botton T, Bastian BC. 2016. CNVkit: genome-wide copy number detection and visualization from targeted DNA sequencing. *PLoS Comput Biol* **12**: e1004873. doi:10.1371/journal.pcbi.1004873
- Tan AY, Manley JL. 2009. The TET family of proteins: functions and roles in disease. *J Mol Cell Biol* **1**: 82–92. doi:10.1093/jmcb/mjp025
- Tardío JC, Machado I, Navarro L, Idrovo F, Sanz-Ortega J, Pellín A, Llombart-Bosch A. 2015. Ewing-like sarcoma with *CIC-DUX4* gene fusion in a patient with neurofibromatosis type 1. A hitherto unreported association. *Pathol Res Pract* **211**: 877–882. doi:10.1016/j.prp.2015.08.003
- Walther MM, Herring J, Enquist E, Keiser HR, Linehan WM. 1999. von Recklinghausen's disease and pheochromocytomas. *J Urol* **162**: 1582–1586. doi:10.1016/S0022-5347(05)68171-2
- Zhang J, Walsh MF, Wu G, Edmonson MN, Gruber TA, Easton J, Hedges D, Ma X, Zhou X, Yergeau DA, et al. 2015. Germline mutations in predisposition genes in pediatric cancer. *N Engl J Med* **373**: 2336–2346. doi:10.1056/NEJMoa1508054
- Zhang N, Liu H, Yue G, Zhang Y, You J, Wang H. 2016. Molecular heterogeneity of Ewing sarcoma as detected by ion torrent sequencing. *PLoS One* **11**: e0153546. doi:10.1371/journal.pone.0153546